LOW-DOSE CT RECONSTRUCTION WITH MULTICLASS ORTHOGONAL DICTIONARIES

Hiryu Kamoshita[†]   *Taisuke Shibata*[†]   *Daichi Kitahara*[†]   *Ken'ichi Fujimoto*[‡]   *Akira Hirabayashi*[†]

[†]Graduate School of Information Science and Engineering, Ritsumeikan University, Shiga, Japan
[‡]Faculty of Engineering and Design, Kagawa University, Kagawa, Japan

ABSTRACT

We propose a high-accuracy CT image reconstruction from low-dose X-ray projection data. A state-of-the-art method exploits dictionary learning for image patches. This method generates an overcomplete dictionary from patches of standard-dose CT images and reconstructs low-dose CT images by minimizing the sum of date fidelity and regularization terms based on sparse representations with the dictionary. However, this method does not take characteristics of each patch into account, such as texture and edges. In this paper, we propose to divide all patches into several classes, and use an individual dictionary with an individual regularization parameter for each class. Moreover, for fast computation, we introduce the orthogonality for each dictionary. Since clustering collects similar patches, accuracy degradation by the orthogonality hardly occurs. Simulation shows the proposed method outperforms the state-of-the-art one in terms of accuracy and speed.

Index Terms— Low-dose CT, image reconstruction, sparse representation, fast dictionary learning, clustering.

1. INTRODUCTION

X-ray computed tomography (CT) is widely used for diagnosis and detection of various diseases because it scans the inside of the human body noninvasively in a few seconds. However the induction of cancerous and genetic diseases by the X-ray radiation is concerned [1]. Hence, it is desired to suppress the X-ray dose to as low as possible. If we apply the standard reconstruction method, *filtered back projection (FBP)*, to low-dose projection data, then large noise and unnatural artifacts appear in the reconstructed image. As a result, we would fail to detect diseased tissues from the reconstructed image [2].

On the basis of the compressed sensing theory [3], we exploit the sparsity to reconstruct a high-quality image from the low-dose projection data. In the image processing field, the patch-based dictionary learning is used to acquire sparse representations of target signals [1], [2], [4]–[8]. A dictionary is generated as a matrix from training images, and a target signal is supposed to be expressed by a linear combination of a few column vectors of the dictionary. In [1], Xu *et al.* combined the patch-based dictionary learning with *statistical iterative reconstruction (SIR)* [9] from the low-dose projection data. Although this method can remove streak artifacts well, detailed structures of the target are lost by over-smoothing. In order to reconstruct the detailed structures while suppressing noise and the artifacts, it is necessary to express each image patch of the target more sparsely.

To obtain more sparse representations, in this paper, we propose to extend the reconstruction method of Xu *et al.* [1] to a multiclass version. In the proposed method, all patches of training images are divided into some classes, and a dictionary is created for each class. Then, patches of the target image are also classified and expressed sparsely by using the dictionary for each class. In this case, it is as-

sumed that the approximation errors, for the patches, of the sparse representations differ depending on the class. Therefore, we propose to use a different regularization parameter for each class. Moreover, for fast reconstruction, we replace the *overcomplete* dictionaries with *orthogonal* matrices. In general, if the number of column vectors of a dictionary is reduced, then the accuracy of each sparse representation degrades, which leads to low-quality reconstructed images. On the other hand, in the proposed method, since a dictionary has only to deal with similar patches due to clustering, the representation accuracy hardly degrades. Simulation using real CT images shows that the proposed method achieves high accuracy and fast computation.

2. SIGNAL MODEL AND DICTIONARY-BASED SIR

In CT, nonnegative attenuation coefficients $\boldsymbol{\mu} \in \mathbb{R}_+^J$ are observed by

$$\boldsymbol{l} = R\boldsymbol{\mu} + \boldsymbol{\xi}, \tag{1}$$

where $R \in \mathbb{R}_+^{I \times J}$ is a Radon transform matrix based on X-ray paths, $\boldsymbol{l} \in \mathbb{R}^I$ is the projection data, and $\boldsymbol{\xi} \in \mathbb{R}^I$ is the observation error. There are two approaches for reducing the X-ray dose: (i) lowering the X-ray intensity and (ii) reducing the number of projections. In the first approach, however, the noise level $\|\boldsymbol{\xi}\|_2$ becomes large. In the second approach, the number I of row vectors of R decreases, which results in $\mathrm{rank}(R) < J$. As a result, in either case, the standard reconstruction method, FBP based on the Fourier slice theorem, generates large noise and unnatural artifacts in the reconstructed images.

Sauer *et al.* proposed a method that reconstructs $\boldsymbol{\mu}$ by maximum a posteriori (MAP) estimation [9]. This method is called SIR since it reconstructs $\boldsymbol{\mu}$ by iteratively minimizing a statistical cost function

$$\|R\boldsymbol{\mu} - \boldsymbol{l}\|_{2,\boldsymbol{w}}^2 + \lambda\Psi(\boldsymbol{\mu}) := \sum_{i=1}^{I} w_i(\boldsymbol{r}_i^{\mathrm{T}}\boldsymbol{\mu} - l_i)^2 + \lambda\Psi(\boldsymbol{\mu}). \tag{2}$$

The weight for the ith projection $\boldsymbol{r}_i^{\mathrm{T}}\boldsymbol{\mu}$ can be statistically defined as $w_i := b/\exp(l_i)$ from the X-ray intensity $b > 0$ and the observed data l_i, $\Psi : \mathbb{R}^J \to \mathbb{R}$ is a regularization term based on *a prior* information on $\boldsymbol{\mu}$, and $\lambda > 0$ is a regularization parameter which controls the balance between the data fidelity and the regularization.

Xu *et al.* combined (2) and the patch-based dictionary learning [1]. In this method, a CT image $\boldsymbol{\mu}$ is decomposed into small images $H_s\boldsymbol{\mu} \in \mathbb{R}^P$ ($s = 1, 2, \ldots, S$), called *patches*, of size $\sqrt{P} \times \sqrt{P}$, where $H_s \in \{0, 1\}^{P \times J}$ is the sth patch extraction matrix and S is the number of the patches. Then, $\boldsymbol{\mu}$ is reconstructed by using an assumption that each patch can be expressed by a linear combination of a few column vectors of an appropriate dictionary $D \in \mathbb{R}^{P \times K}$, where K is the number of column vectors $\boldsymbol{d}_k \in \mathbb{R}^P$ s.t. $\|\boldsymbol{d}_k\|_2 = 1$ ($k = 1, 2, \ldots, K$). By defining $\boldsymbol{c}_s \in \mathbb{R}^K$ as sparse representations (coefficients) for $H_s\boldsymbol{\mu}$, this method solves the following problem

$$\underset{\boldsymbol{\mu},(D),C}{\mathrm{minimize}} \|R\boldsymbol{\mu} - \boldsymbol{l}\|_{2,\boldsymbol{w}}^2 + \lambda\sum_{s=1}^{S}(\|H_s\boldsymbol{\mu} - D\boldsymbol{c}_s\|_2^2 + \nu_s\|\boldsymbol{c}_s\|_0), \tag{3}$$

where $C := (\boldsymbol{c}_1, \boldsymbol{c}_2, \dots, \boldsymbol{c}_S) \in \mathbb{R}^{K \times S}$ and $\nu_s > 0$ is a Lagrangian multiplier for each patch. On (3), there are two cases where (i) D is fixed to a matrix pre-learned from training images, and (ii) D is adaptively updated by using the estimated target image $\boldsymbol{\mu}$. The former and the latter are called *global dictionary-based SIR (GDSIR)* and *adaptive dictionary-based SIR (ADSIR)*, respectively.

Since it is difficult to directly solve the optimization problem in (3), the sparse coefficient C (& the dictionary D) and the CT image $\boldsymbol{\mu}$ are alternately updated from the initial image $\boldsymbol{\mu}^0$ obtained by the FBP. The matrix C (and D) is updated by solving the problem

$$\underset{(D),C}{\text{minimize}} \sum_{s=1}^{S} (\|H_s \boldsymbol{\mu}^{m-1} - D\boldsymbol{c}_s\|_2^2 + \nu_s \|\boldsymbol{c}_s\|_0), \qquad (4)$$

where $\boldsymbol{\mu}$ is fixed to the estimated value $\boldsymbol{\mu}^{m-1}$. In GDSIR, only C is updated by *orthogonal matching pursuit (OMP)* [10]. In ADSIR, after updating D by an online learning algorithm in [11], C is updated by OMP. Hence ADSIR requires a lot of computational time compared to GDSIR. The image $\boldsymbol{\mu}$ is updated by solving the problem

$$\underset{\boldsymbol{\mu} \in \mathbb{R}_+^J}{\text{minimize}} \|R\boldsymbol{\mu} - \boldsymbol{l}\|_{2,\boldsymbol{w}}^2 + \lambda \sum_{s=1}^{S} \|H_s \boldsymbol{\mu} - D\boldsymbol{c}_s\|_2^2 \qquad (5)$$

with fixed C (and D). For the problem in (5), GDSIR and ADSIR use the majorization-minimization (MM) [12] to avoid the computation of a large inverse matrix. Specifically, $\boldsymbol{\mu}$ is updated from the previous one $\boldsymbol{\mu}^{m-1}$ as in (6), where $W := \text{diag}(\boldsymbol{w})$, $\boldsymbol{0}$ & $\boldsymbol{1}$ are respectively vectors whose all components are 0 & 1, $\oslash$ is the component-wise division, and $\max$ returns a larger value in each component [13].

3. SIR WITH MULTICLASS DICTIONARY LEARNING

Recently, in the high-speed MRI and low-dose CT fields, image reconstructions with multiclass dictionary learning have been proposed for higher compression ratio, noise reduction, and artifact suppression [2], [7], [8]. In these methods, image patches are classified into multiple classes by using geometric directions or pixel values. Then, since dictionaries are generated for each class, the accuracy of sparse representations for the patches is improved, which leads to good reconstruction results. The methods in [7], [8] are proposed for high-speed MRI and hence cannot be directly applied to low-dose CT. The method in [2] uses the $\|\boldsymbol{\mu} - \boldsymbol{\mu}^0\|_2^2$ as the data fidelity term, and hence the reconstruction results depend largely on $\boldsymbol{\mu}^0$ obtained by the FBP.

On the other hand, since GDSIR uses $\|R\boldsymbol{\mu} - \boldsymbol{l}\|_{2,\boldsymbol{w}}^2$ as the data fidelity term, the reconstruction results are robust against the initial image $\boldsymbol{\mu}^0$. Therefore, in this paper, we propose to extend GDSIR to a multiclass version in order to reconstruct higher-quality CT images.

3.1. Multiclass GDSIR

Let Q be the number of classes and $q = 1, 2, \dots, Q$ be the index of the class. A dictionary $D_q \in \mathbb{R}^{P \times K_q}$ for the qth class is generated in advance from standard-dose images, where K_q is the number of column vectors of D_q. Patches $H_s \boldsymbol{\mu}$ of a target image are classified, and we define $\mathcal{S}_q$ s.t. $\bigcup_{q=1}^{Q} \mathcal{S}_q = \{1, 2, \dots, S\}$ and $\mathcal{S}_q \cap \mathcal{S}_{q'} = \varnothing$ ($q \neq q'$) as a patch index set for the qth class. We reconstruct $\boldsymbol{\mu}$ by solving

$$\underset{\boldsymbol{\mu}, C}{\text{minimize}} \|R\boldsymbol{\mu} - \boldsymbol{l}\|_{2,\boldsymbol{w}}^2 + \sum_{q=1}^{Q} \lambda_q \sum_{s \in \mathcal{S}_q} (\|H_s \boldsymbol{\mu} - D_q \boldsymbol{c}_s\|_2^2 + \nu_s \|\boldsymbol{c}_s\|_0)$$
$$(7)$$

which is a multiclass version of (3). Note that here we use a different regularization parameter $\lambda_q > 0$ for each class. By fixing the sets $\mathcal{S}_q$, the problem in (7) can be solved by a similar update to that of GDSIR.

Moreover, to reduce the computational time, we propose to introduce orthogonal dictionaries $\widehat{D}_q \in \mathbb{R}^{P \times P}$ s.t. $\widehat{D}_q^{\mathrm{T}} \widehat{D}_q = E$ to (7), where E is the identity matrix of order P. In general, if an overcomplete dictionary is replaced with an orthogonal matrix, then calculation speed increases but the accuracy of each sparse representation degrades. On the other hand, in the proposed method, since similar patches are collected by clustering, the degradation of the representation accuracy hardly occurs even if we use orthogonal dictionaries.

3.2. The Proposed Reconstruction Algorithm

The proposed algorithm reconstructs $\boldsymbol{\mu}$ from the initial estimate $\boldsymbol{\mu}^0$ by alternately executing the sparse coefficient update step and the image update step M times after executing the preparation one time.

Preparation: First, patches are extracted from training images and classified into Q classes by K-means algorithm in the same manner as [8]. To also classify patches of the target images later, we store the clustering centers. Then, an orthogonal dictionary $\widehat{D}_q$ is created for each class as an approximate solution to the optimization problem

$$\underset{\widehat{D}_q, C_q^{\mathrm{tr}}}{\text{minimize}} \sum_{s \in \mathcal{S}_q^{\mathrm{tr}}} (\|H_s \boldsymbol{\mu}^{\mathrm{tr}} - \widehat{D}_q \boldsymbol{c}_s^{\mathrm{tr}}\|_2^2 + \nu_s \|\boldsymbol{c}_s^{\mathrm{tr}}\|_0) \quad \text{s.t. } \widehat{D}_q^{\mathrm{T}} \widehat{D}_q = E,$$
$$(8)$$

where $\boldsymbol{\mu}^{\mathrm{tr}}$ is a standard-dose training image, $\boldsymbol{c}_s^{\mathrm{tr}}$ is a sparse coefficient vector for the sth training patch $H_s \boldsymbol{\mu}^{\mathrm{tr}}$, $\mathcal{S}_q^{\mathrm{tr}}$ is a patch index set for the training patches of class q. For solving the problem in (8), we alternately update $\widehat{D}_q$ and C_q^{tr} according to [5]. By fixing C_q^{tr} in (8), $\widehat{D}_q$ is updated as.

$$\widehat{D}_q^* = \underset{\widehat{D}_q}{\text{argmin}} \|\Phi_q^{\mathrm{tr}} - \widehat{D}_q C_q^{\mathrm{tr}}\|_{\mathrm{F}}^2 \quad \text{s.t. } \widehat{D}_q^{\mathrm{T}} \widehat{D}_q = E, \qquad (9)$$

where $\Phi_q^{\mathrm{tr}} \in \mathbb{R}^{P \times |\mathcal{S}_q^{\mathrm{tr}}|}$ is the matrix whose column vectors are the training patches of class q, i.e., $H_s \boldsymbol{\mu}^{\mathrm{tr}}$ ($s \in \mathcal{S}_q^{\mathrm{tr}}$), and $\|\cdot\|_{\mathrm{F}}$ denotes the Frobenius norm. The problem in (9) is known as the *orthogonal Procrustes problem* [3], and hence the solution is given by.

$$\widehat{D}_q^* = UV^{\mathrm{T}} \qquad (10)$$

with the use of the singular value decomposition $\Phi_q^{\mathrm{tr}} C_q^{\mathrm{trT}} = U\Sigma V^{\mathrm{T}}$. Then, by fixing $\widehat{D}_q$ in (8), C_q^{tr} is updated as

$$C_q^{\mathrm{tr}*} = \underset{C_q^{\mathrm{tr}}}{\text{argmin}} \sum_{s \in \mathcal{S}_q^{\mathrm{tr}}} (\|H_s \boldsymbol{\mu}^{\mathrm{tr}} - \widehat{D}_q \boldsymbol{c}_s^{\mathrm{tr}}\|_2^2 + \nu_s \|\boldsymbol{c}_s^{\mathrm{tr}}\|_0). \quad (11)$$

From the property of $\widehat{D}_q^{\mathrm{T}} \widehat{D}_q = E$, the solution to (11) is quickly computed for each column vector $\boldsymbol{c}_s^{\mathrm{tr}*}$ ($s \in \mathcal{S}_q^{\mathrm{tr}}$) by

$$\boldsymbol{c}_s^{\mathrm{tr}*} = \text{Hard}_{\nu_s}(\widehat{D}_q^{\mathrm{T}} H_s \boldsymbol{\mu}^{\mathrm{tr}}) \qquad (12)$$

with the use of the hard thresholding operator

$$\text{Hard}_\nu(\boldsymbol{c})[i] = \begin{cases} \boldsymbol{c}[i] & \text{if } |\boldsymbol{c}[i]| \geq \sqrt{\nu}, \\ 0 & \text{if } |\boldsymbol{c}[i]| < \sqrt{\nu}, \end{cases}$$

where $[i]$ denotes the ith component of a vector. By repeating (10)

$$\boldsymbol{\mu}^m = \max \left\{ \boldsymbol{0}, \boldsymbol{\mu}^{m-1} - \left[R^{\mathrm{T}} W (R\boldsymbol{\mu}^{m-1} - \boldsymbol{l}) + \lambda \sum_{s=1}^{S} H_s^{\mathrm{T}} (H_s \boldsymbol{\mu}^{m-1} - D\boldsymbol{c}_s) \right] \oslash \left[\left(R^{\mathrm{T}} W R + \lambda \sum_{s=1}^{S} H_s^{\mathrm{T}} H_s \right) \boldsymbol{1} \right] \right\} \qquad (6)$$

and (12) until a convergence condition is satisfied, $\widehat{D}_q$ is generated.

To solve (7) with the multiclass orthogonal dictionaries $\widehat{D}_q$, first, the initial estimate $\boldsymbol{\mu}^0$ is obtained by applying the FBP to the low-dose projection data $\boldsymbol{l}$. Then, by using the stored clustering centers in the preparation, the initial patches $H_s\boldsymbol{\mu}^0$ are classified into Q classes by the nearest neighbor method, and hereafter the patch index sets $\mathcal{S}_q$ are fixed. We reconstruct a target CT image $\boldsymbol{\mu}$ by repeating the sparse coefficient update and image update steps for $m = 1, 2, \ldots, M$.

Sparse Coefficient Update Step: At the mth update of C, in the same manner as (12), each column vector $\boldsymbol{c}_s$ is updated by

$$\boldsymbol{c}_s = \mathrm{Hard}_{\nu_s}(\widehat{D}_{q(s)}^{\mathrm{T}} H_s \boldsymbol{\mu}^{m-1}), \tag{13}$$

where $\boldsymbol{\mu}$ is fixed to the estimated value $\boldsymbol{\mu}^{m-1}$ and $q(s)$ denotes the class of the sth patch. Differently from the problem in (4), since we use the orthogonal dictionaries, we can quickly compute the exact closed form solution as shown in (13) without using OMP.

Image Update Step: At the mth update of $\boldsymbol{\mu}$, we solve the problem

$$\underset{\boldsymbol{\mu} \in \mathbb{R}_+^J}{\mathrm{minimize}} \ \|R\boldsymbol{\mu} - \boldsymbol{l}\|_{2,\boldsymbol{w}}^2 + \sum_{q=1}^{Q} \lambda_q \sum_{s \in \mathcal{S}_q} \|H_s\boldsymbol{\mu} - \widehat{D}_q \boldsymbol{c}_s\|_2^2 \tag{14}$$

with fixed C. For the problem in (14), by using the same MM technique as [13], $\boldsymbol{\mu}$ is updated from the previous one $\boldsymbol{\mu}^{m-1}$ as in (15).

3.3. Importance of the Regularization Parameters λ_q

In multiclass dictionary learning, the number of patches is different for each class. In addition, there is a possibility that the ratio of the number of patches in each class is quite different between the training image and the target image. As a result, the approximation errors of the sparse representations by dictionaries differ depending on the class. In order to obtain better reconstruction results, it is desirable to set Lagrangian multipliers ν_s (and the numbers of column vectors K_q if overcomplete dictionaries are used) to different values for each class. However, it becomes difficult to achieve uniform representation accuracy among all classes as the number of classes increases.

For avoiding the above problem, in the proposed method, we also extend the regularization parameter λ in (3) to the multiclass ones λ_q in (7). This extension allows us to reconstruct high-quality images by appropriate tuning of each λ_q even if we set ν_s to the same value for all classes. Specifically, we only have to set λ_q to a large value for a class where the representation accuracy is high, and set λ_q to a small value for a class where the representation accuracy is low.

4. NUMERICAL SIMULATION

In this section, we show the effectiveness of the proposed method in (7) with overcomplete (Proposed 1) and orthogonal (Proposed 2) dictionaries by numerical simulation based on actual CT images in [14]. We used a female head image f_1601 as a training image and used female head images f_1610 & f_1615 and male head images m_1114 & m_1132 as target images. All image sizes were 256×256 ($J = 65,536$). We created attenuation coefficients $\boldsymbol{\mu}$ from CT values with the attenuation coefficient of water $\mu_{\mathrm{water}} = 0.2059\,[\mathrm{cm}^{-1}]$. In (1), a Radon transform matrix was created on the basis of parallel pencil beams to 367 X-ray detectors in 60 views $\theta_g = 3(g-1)\,[\mathrm{deg}]$ ($g = 1, 2, \ldots, 60$ and $I = 22{,}020$), where we assumed that the width and

(a) Training image (f_1601). (b) Clustering centers and λ_q.
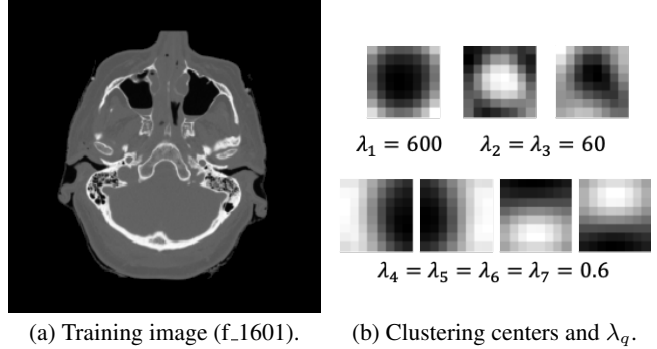
Fig. 1. Training image for dictionary leaning and clustering centers.

Table 1. PSNR [dB] and the calculation time [sec] for each method.

Method \ No.	f_1610	f_1615	m_1114	m_1132	calc. time
GDSIR	32.32	32.36	33.45	32.02	0.60/iter.
ADSIR	32.20	32.23	33.36	31.92	4.04/iter.
Proposed 1	**36.08**	36.50	36.82	35.00	0.67/iter.
Proposed 2	35.95	**36.57**	**36.96**	**35.11**	**0.46**/iter.

height of one pixel were $0.09\,[\mathrm{cm}]$ and X-ray intensity was $b = 10^6$.

In all methods (GDSIR, ADSIR, and Proposed 1 & 2), we reconstructed images by $M = 1{,}000$ iterations and fixed parameters $K = 256$ (for overcomplete dictionaries) and $\nu_s = 0.2$. For overcomplete dictionaries, we used the program in [15] for fast implementation of dictionary learning and OMP. We extracted $S = 62{,}001$ patches of size 8×8 ($P = 64$) by shifting the areas pixel by pixel. Dictionaries of GDSIR and Proposed 1 & 2 were learned from the training image in Fig. 1(a). In Proposed 1 & 2, we divided the training patches into $Q = 7$ classes, which could achieve the highest PSNR among $Q \in \{2, 3, \ldots, 16\}$, and each clustering center was given as in Fig. 1(b). We set the regularization parameters to $\lambda = 60$ in GDSIR & ADSIR and $\lambda_1 = 600, \lambda_2 = \lambda_3 = 60, \lambda_4 = \lambda_5 = \lambda_6 = \lambda_7 = 0.6$ in Proposed 1 & 2. The simulation environment was MacBook Pro, OS Mojave ver. 10.14, CPU 3.1 GHz Intel Core i5, and memory 8 GB 2133 MHz LPDDR3, where platform was MATLAB R2018a 64-bit.

Table 1 summarizes PSNR of the reconstructed images and the calculation time per one iteration for each method. In Figs. 2 and 3, (a), (b), (c), (d), (e), and (f) show the original image, the initial estimate $\boldsymbol{\mu}^0$ obtained by the FBP, the reconstructed images by GDSIR, ADSIR, Proposed 1, and Proposed 2 for f_1615 & m_1132, respectively. From Table 1, we found that Proposed 2 achieved both of high reconstruction accuracy and fast computation. From Figs. 2 and 3, we found that GDSIR & ADSIR lost detailed structures by over-smoothing while Proposed 1 & 2 could reconstruct the detailed structures.

5. CONCLUSION

In this paper, we proposed a low-dose CT reconstruction using multiclass dictionary learning. Since the propose method performs clustering for patches of a target only once, the computational cost hardly increases from GDSIR. Moreover, by introducing multiclass regularization parameters and orthogonal dictionaries, the proposed method can achieve high accuracy and fast computation. Simulation showed that the proposed method reconstructs detailed structures of targets.

$$\boldsymbol{\mu}^m = \max\left\{\boldsymbol{0}, \boldsymbol{\mu}^{m-1} - \left[R^{\mathrm{T}}W(R\boldsymbol{\mu}^{m-1} - \boldsymbol{l}) + \sum_{q=1}^{Q}\lambda_q \sum_{s \in \mathcal{S}_q} H_s^{\mathrm{T}}(H_s\boldsymbol{\mu}^{m-1} - \widehat{D}_q\boldsymbol{c}_s)\right] \oslash \left[\left(R^{\mathrm{T}}WR + \sum_{q=1}^{Q}\lambda_q \sum_{s \in \mathcal{S}_q} H_s^{\mathrm{T}}H_s\right)\boldsymbol{1}\right]\right\} \tag{15}$$
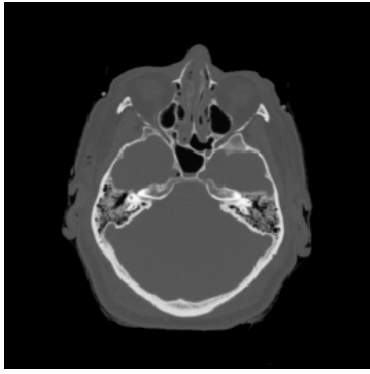
(a) Original image (f_1615).
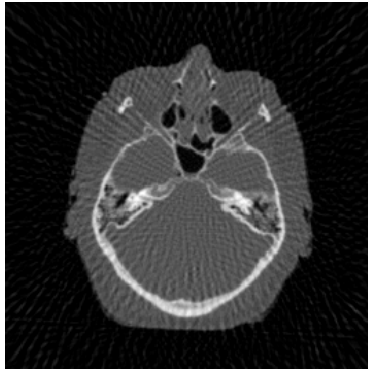
(b) Initial estimate by the FBP.
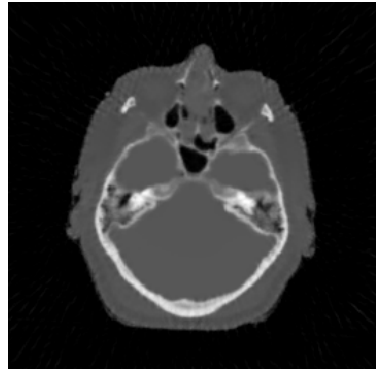
(c) GDSIR [32.26 / 0.859].
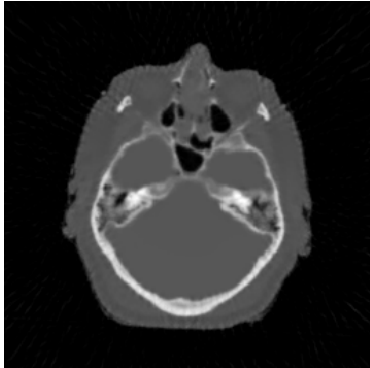
(d) ADSIR [32.23 / 0.855].
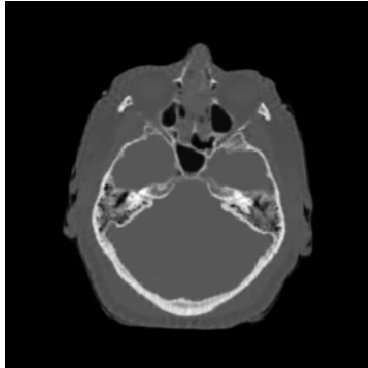
(e) Proposed 1 [36.50 / **0.979**].
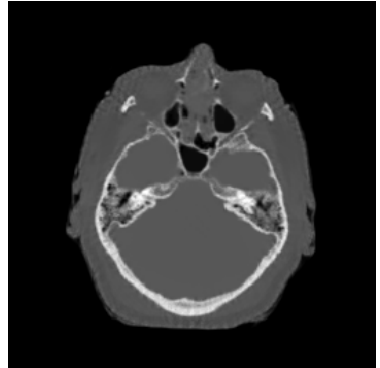
(f) Proposed 2 [**36.57** / 0.978].

Fig. 2. Reconstruction results of f_1615 from its low-dose projection data by each method [PSNR / SSIM].
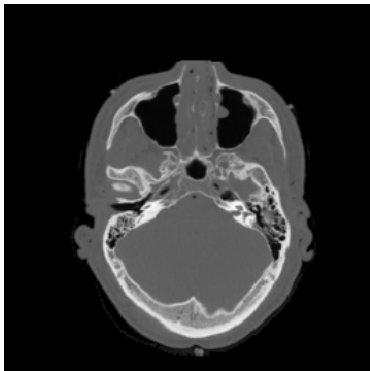
(a) Original image (m_1132)
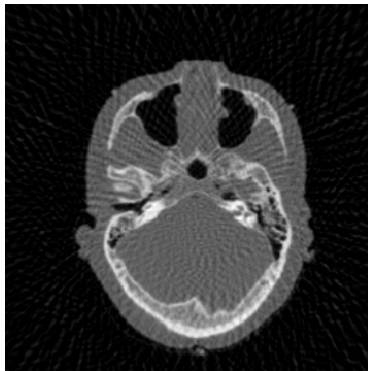
(b) Initial estimate by the FBP.
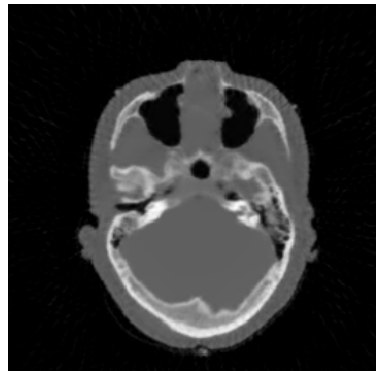
(c) GDSIR [32.02 / 0.843].
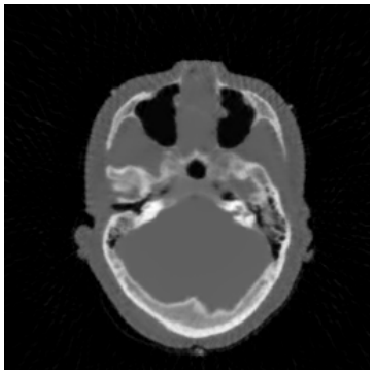
(d) ADSIR [31.92 / 0.840].
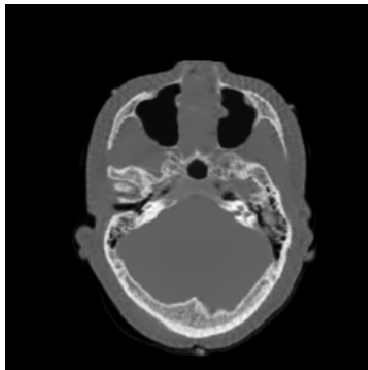
(e) Proposed 1 [35.00 / **0.969**].
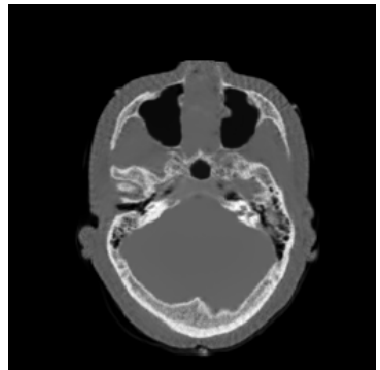
(f) Proposed 2 [**35.11** / **0.969**].

Fig. 3. Reconstruction results of m_1132 from its low-dose projection data by each method [PSNR / SSIM].

6. REFERENCES

[1] Q. Xu, H. Yu, X. Mou, L. Zhang, J. Hsieh, and G. Wang, "Low-dose X-ray CT reconstruction via dictionary learning," *IEEE Transactions on Medical Imaging*, vol. 31, no. 9, pp. 1682–1697, 2012.

[2] Y. Chen, L. Shi, Q. Feng, J. Yang, H. Shu, L. Luo, J. L. Coatrieux, and W. Chen, "Artifact suppressed dictionary learning for low-dose CT image processing," *IEEE Transactions on Medical Imaging*, vol. 33, no. 12, pp. 2271–2292, 2014.

[3] M. Elad, *Sparse and Redundant Representations: From Theory to Applications in Signal and Image Processing*. New York, NY: Springer, 2010.

[4] Y. Chen, X. Yin, L. Shi, H. Shu, L. Luo, J. L. Coatrieux, and C. Toumoulin, "Improving abdomen tumor low-dose CT images using a fast dictionary learning based processing," *Physics in Medicine and Biology*, vol. 58, no. 16, pp. 5803–5820, 2013.

[5] C. Bao, J. F. Cai, and H. Ji, "Fast sparsity-based orthogonal dictionary learning for image restoration," in *Proceedings of 2013 IEEE International Conference on Computer Vision (ICCV)*, 2013, pp.3384–3391.

[6] C. Zhang, T. Zhang, M. Li, C. Peng, Z. Liu, and J. Zheng, "Low-dose CT reconstruction via ℓ_1 dictionary learning regularization using iteratively reweighted least-squares," *Biomedical Engineering Online*, vol. 15, no. 66, pp. 1–21, 2016.

[7] Z. Zhan, J. F. Cai, D. Guo, Y. Liu, Z. Chen, and X. Qu, "Fast multiclass dictionaries learning with geometrical directions in MRI reconstruction," *IEEE Transactions on Biomedical Engineering*, vol. 63, no. 9, pp. 1850–1861, 2016.

[8] N. Inamuro, M. Shibata, C. Tang, T. Ijiri, and A. Hirabayashi, "High-quality MR imaging based on dictionary learning using training images and observed signals," *IEICE Technical Report (in Japanese)*, vol. 116, no. 395, pp. 123–128, 2017.

[9] K. Sauer and C. Bouman, "A local update strategy for iterative reconstruction from projections," *IEEE Transactions on Signal Processing*, vol. 41, no. 2, pp. 534–548, 1993.

[10] Y. C. Pati, R. Rezaiifar, and P. S. Krishnaprasad, "Orthogonal matching pursuit: Recursive function approximation with applications to wavelet decomposition," in *Conference Record of The Twenty-Seventh Asilomar Conference on Signals, Systems and Computers*, 1993, pp. 40–44.

[11] J. Mairal, F. Bach, J. Ponce, and G. Sapiro, "Online learning for matrix factorization and sparse coding," *Journal of Machine Learning Research*, vol. 11, pp. 19–60, 2010.

[12] D. R. Hunter and K. Lange, "Quantile regression via an MM algorithm," *Journal of Computational and Graphical Statistics*, vol. 9, no. 1, pp. 60-77, 2000.

[13] I. A. Elbakri and J. A. Fessler, "Statistical image reconstruction for polyenergetic X-ray computed tomography," *IEEE Transactions on Medical Imaging*, vol. 21, no. 2, pp. 89–99, 2002.

[14] Magnetic Resonance Research Facility, *Visible Human Project CT Datasets*. [Online] https://medicine.uiowa.edu/mri/facility-resources/images/visible-human-project-ct-datasets

[15] J. Mairal, J. P. Chieze, Y. Chen, G. Durif, R. Jenatton, F. Bach, J. Ponce, G. Obozinski, B. Yu, G. Sapiro, and Z. Harchaoui, *Spams: a SPArse Modeling Software ver. 2.6*. [Online] http://spams-devel.gforge.inria.fr/doc/html